WHERE HAVE ALL THE RINGS GONE? EXPLORING THE REPUTED MULTIRING NATURE OF MERCURY'S CALORIS BASIN. G. J. Gosselin[1]*, A. M. Freed[1], and B. C. Johnson[1,2], [1]Dept. of Earth, Atmospheric, and Planetary Sciences, Purdue University, West Lafayette, IN 47907, [2]Dept. of Physics and Astronomy, Purdue University *(ggosseli@purdue.edu)

Introduction: The ~1550 km diameter Caloris basin is Mercury's largest, oldest, and best-preserved impact basin [1-3]. Ever since Mariner 10's first glimpse of the massive impact structure, it has been suggested that Caloris is a multiring basin [e.g., 4, 5], though whether these rings exist remains an open question [2]. The subsequent MESSENGER mission resulted in the adjustment or refutation of the initial proposed ring locations, in addition to the identification of several new potential ring locations. In total, post-MESSENGER analyses [1, 6-8] account for a reported seven potential basin-interior rings with radii 315, 350, 450, 500, 540, 640, and 690 km, and two exterior to the basin rim with radii of 850 and 1010 km, all of which are likely buried beneath post-Caloris volcanic flows of variable thickness [e.g., 2, 6].

Based upon the success of previous models to simultaneously match the observed crustal thickness distribution and ring locations of lunar multiring basins [9, 10], we explore the possibility of ring formation during the formation of Caloris. Here we present the preliminary results from a suite of numerical impact simulations, constrained by the observed basin diameter and crustal thickness data from MESSENGER [11], that highlight regions of localized plastic strain. As with the lunar studies, our models utilize calculated regions of localized shear to identify possible basin rings [9, 10]. If rings were found to form in the models, their predicted locations were compared against the radii from the aforementioned observational studies.

Methods: The iSALE-2D shock physics code [12-14] was used to simulate the formation of Caloris basin on a Mercury-like target. We considered impactors with diameters (D_{imp}) of 100, 120, and 140 km traveling at 42 km/s [15], and lithospheric thermal gradients (dT/dz) of 10, 20, and 30 K/km that became adiabatic upon reaching 1400 K. All models assumed an axisymmetric spherical geometry with a central gravity field. Following [11], we assume Mercury's silicate layers consist of a 35 km thick basaltic crust and 365 km thick dunite mantle [11]. A spatial resolution of 1 km was used within a high-resolution zone that encompassed the final basin's radius. Strength and rheological models used by [9, 10] were also implemented. Candidate ring locations were identified by locating regions of plastic strain accumulation (ε_p).

Preliminary Results: Our best-fitting models, those that match the observed crustal thickness distribution, assumed impactor diameters of 100 or 120 km, and a thermal gradient of 30 K/km (Fig. 1). One of our best-fit simulations (D_{imp} = 100 km) shows some correlation with the proposed ring 850 km from the basin center [7], but it is not the sole basin-exterior normal fault predicted by the model; at least two other possible faults reside at 825 and 915 km (see Fig. 2c). While zones of localized deformation occur near the proposed ring locations, it is not readily apparent that they are indeed ring faults as extensional failure alone cannot explain the observed deformation.

Formation mechanisms. The first localized shear zones to breach the surface occur between 600-800 km from the basin center as the central uplift drags material inward from distances far greater than the now extant transient crater's rim (R ≈ 350) causing extensional failure throughout the entirety of the crust (Fig. 2a). This inward flow is owed to the warmer and weaker underlying mantle material which exerts a basal drag force on the base of the crust [16]. Outward flowing inner crust (< 500 km from center of basin) is overthrust by inward flowing outer crust (> 500 km from center of basin) causing the crust to fold and thicken under the resultant compressive stresses (Fig. 2a).

Continued collapse of the central uplift further modifies the extensional zone seen in Figure 2a as another compressive episode compacts and uplifts material between 500-700 km (Fig. 2b). This serves to thicken the previously extended crust. Extensional failure, however, dominates outside of 700 km from the impact site which localizes plastic strain at 825, 865, and 915 km (Fig. 2b). Three discrete crustal blocks form within the innermost 500 km of the basin. Each crustal block is ~100 km wide and forms as a result of repeated thrusting

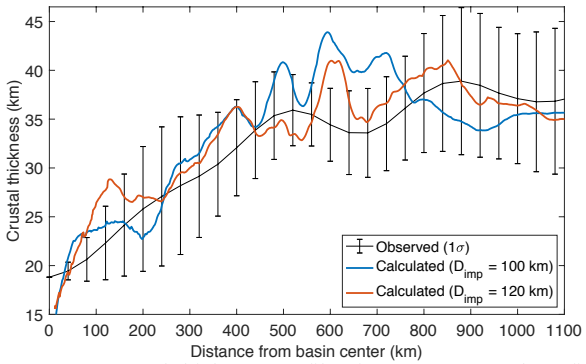

Figure 1. Crustal thickness profiles from our current best-fit models assuming dT/dz = 30 K/km compared to the azimuthally averaged observed [9] crustal thickness distribution. Error bars denote one standard deviation from the mean.

and extension (Fig. 2b). As dynamic motion (i.e., topographic undulations > 10 km) ceases, a final period of extension occurs within the lithosphere. Localized shearing takes place along the boundaries separating the crustal blocks (Fig. 2c) evidenced by the local maxima of ε_p.

Discussion: Our model shown in Figure 2c predicts regions of localized plastic strain at basin-radial distances of 340, 465, 555, 660, 755 km within the present-day basin rim and 825, 865, and 915 km outside the basin rim. While the localized deformation zones inside of ~750 km are not basin rings in the classical sense [e.g., 16], they do appear to correspond to local minima of crustal thickness (Fig. 1) which roughly coincide with presumed ring locations. The large crustal blocks produced by our simulations have also been observed in other models of basin forming impacts where similar crustal "boudinage" was reported [17]; thus, they are not unique to Mercurian-like targets.

The calculated basin's rim resides at ~865 km (Fig. 2c), 90 km larger than the reported value [1], despite its ability to match the observed crustal thickness. We also note that the other best-fit model (D_{imp} = 120 km) provides a better match to the observed crustal thickness distribution, especially within 450-750 km of the basin's center (Fig. 1). The location of its rim, however, (> 1000 km) also yields a basin far larger than Caloris' suggested dimensions [1]. Nonetheless, it is still intriguing that our model produces localized strains at the approximate locations of purported rings by simply matching the observed crustal thickness distribution.

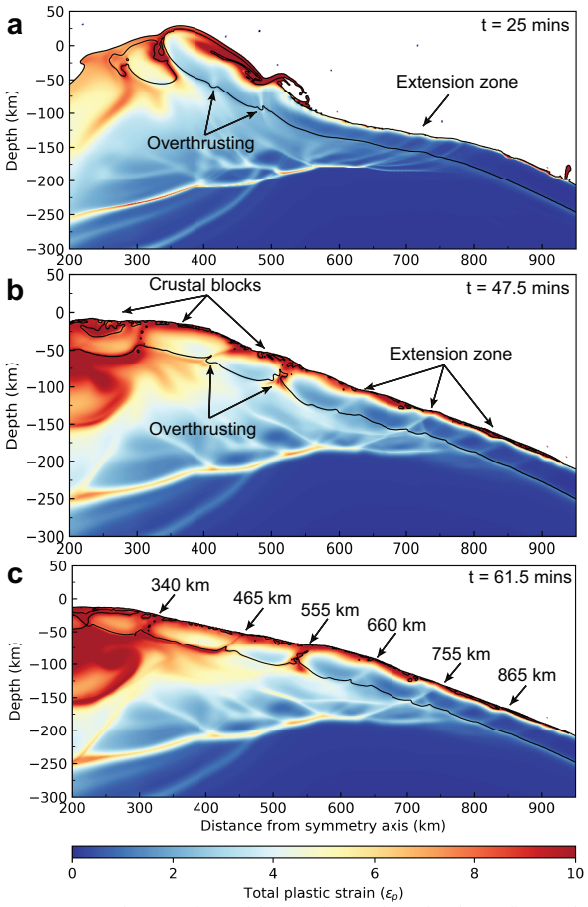

Figure 2. Time series of basin formation for best fit model with D_{imp} = 100 km. Materials are colored according to their total plastic strain accumulation and separated by thin black curves. Inner 200 km of the basin have been omitted for clarity.

According to [6, 8], a buried basin ring with a radius of 450 km may exert some control on the transition from basin-radial to -circumferential faulting within Caloris' interior volcanic plains; thus, the underlying surface morphology of the originally empty basin may play a role in the evolution of the stress-state within the superposed volcanic fill in a similar manner to smaller volcanically buried craters in Mercury's northern volcanic plains [18].

Future Work: In the near term, we intend to broaden our parameter space by including additional impactor diameters and velocities, pre-impact crustal thicknesses, and thermal profiles; the latter have shown to exert a strong control on the location and relative spacing between ring faults [10]. Given the several kilometers of volcanic fill within Caloris, we also plan on implementing these results within a finite element solver to further investigate the hypothesis that buried basin rings exert a control on the location of observed faulting at the volcanic surface [6, 8].

Acknowledgments: We gratefully thank the developers of iSALE including Gareth Collins, Kai Wünneman, Dirk Elbeshausen, Boris Ivanov, Tom Davison, and Jay Melosh. This work is supported by the NSF GRFP (DGE-1842166).

References: [1] Fassett C. I. et al. (2009) *EPSL*, *285*, 297-308. [2] Fassett C. I. et al. (2012) *JGR*, *117*, E00L08. [3] Murchie S. L. et al. (2008) *Science*, *321*, 73-76. [4] Strom R. G. et al. (1975) *JGR*, *80*, 2478-2507. [5] Spudis P. D. and Guest J. E. (1988) *Mercury*. [6] Byrne P. K. et al. (2018) *Mercury: The View after MESSENGER*. [7] Oberst J. et al. (2010) *Icarus*, *209*, 230-238. [8] Cunje A. B. and Ghent R.R. (2016) *Icarus*, *268*, 131-144. [9] Johnson B. C. et al. (2016) *Science*, *354*, 441-444. [10] Johnson B. C. et al. (2018) *JGRP*, *123*, 3035-3050. [11] Genova A. et al. (2019) *GRL*, *46*, 1-25. [12] Amsden A. et al. (1980) *LANL Report*, *8095*, 101p. [13] Collins G. S. et al. (2004) *Meteor. and Planet. Sci*., *39*, 217-231. [14] Wünnemann K. et al. (2006) *Icarus*, *180*, 514-527. [15] Le Feuvre M. and Wieczorek M. A. (2008) *Icarus*, *197*, 291-306. [16] Melosh H. J. and McKinnon W. B. (1978) *GRL*, *5*, 985-988. [17] Trowbridge A. J. et al. (2020) *Icarus*, *352*, 113995. [18] Freed A. M. et al. (2012) *JGR*, *117*, E00L06.